A Wireless Communication System for Urban Water Supply Networks Based on Guided Acoustic Waves

IEEE Access
Multidisciplinary ⋮ Rapid Review ⋮ Open Access Journal

Received 20 September 2022, accepted 7 October 2022, date of publication 12 October 2022, date of current version 18 October 2022.

Digital Object Identifier 10.1109/ACCESS.2022.3213973

RESEARCH ARTICLE

A Wireless Communication System for Urban Water Supply Networks Based on Guided Acoustic Waves

MARKELJAN FISHTA, (Member, IEEE), ERICA RAVIOLA, (Member, IEEE), AND FRANCO FIORI, (Member, IEEE)
Department of Electronics and Telecommunication, Politecnico di Torino, 10129 Turin, Italy
Corresponding author: Franco Fiori (franco.fiori@polito.it)

This work was supported in part by IREN S.p.A - Direzione Innovazione - Reggio Emilia, Italy.

ABSTRACT The structural complexity of real-world pipeline networks makes it difficult to derive physics-based models of acoustic propagation. This work deals with the design of a communication system based on the propagation of acoustic waves in water-filled pipes. A method based on the experimental characterization of the communication channel is proposed. This approach is applied to an urban water distribution pipeline, and a black-box model representing its frequency response is obtained. The derived two-port model is used for the simulation of a complete communication system, comprising transmitter and receiver models, with the aim of using the water pipe as a wireless communication channel. It is shown that the choice of modulation parameters is critical in order to deal with issues such as the frequency selectivity of the channel and multipath wave propagation. A communication system is presented and the experimental results of the communicated data are provided.

INDEX TERMS Acoustic wave communication, channel characterization, data transmission, underwater communication, urban water supply system.

I. INTRODUCTION

Communication systems based on non conventional channels are increasingly used, mostly in industrial environments. They provide an alternative for data transmission in scenarios where traditional wireless or wired channels cannot be used because they are unavailable or ineffective. Prior research has investigated the use of media ranging from soil [1], [2] and a lifeline cable [3] in mining environments, to pipes meant for the transportation of water, gas or oil [4], [5], [6], [7]. Applications include, but are not limited to, systems for communication in the post-accident scenario, structural health monitoring and tracking of the operating conditions of an industrial plant.

Recently, in-pipe data transmission has acquired increasing interest from researchers, since Urban Water Supply Systems (UWSSs) provide a readily available infrastructure made of pipes, which has a large spatial extension and can reach areas not covered by traditional communication infrastructures.

Four major communication methods can be identified for the underwater case, including radio frequency (RF), free-space optical (FSO), magnetic induction (MI) and acoustic wave (AW) [8]. Among these, RF is not suitable for use in underground environments due to its absorption by the soil while FSO is vulnerable to absorption, scattering and dispersion, and is affected by the turbidity of the water [9]. AW has become the most popular due to its ability to overcome the above mentioned issues and reach over a long propagation distance [10].

In the last decades, extensive research has focused on acoustic underwater communication, which poses great challenges due to its characteristics of multipath propagation, band limitation and reduced speed [11], [12], [13]. Open sea acoustic channels are classified as horizontal or vertical and as shallow or deep sea [12]. In shallow and horizontal channels the main reason for signal distortion is reflection from the bottom and the surface of the sea, while in vertical

The associate editor coordinating the review of this manuscript and approving it for publication was Fang Yang.

and deep sea channels, ray bending due to changes in the propagation speed with depth, produces the dominant effect. Furthermore, the channel characteristics vary with time and are highly dependent on the location of the transmitter and the receiver as well.

Reverberation can result in time spreading, amplitude and phase distortion and frequency shifting [12], [14], [15]. Countermeasures such as beam-steering, focusing, or phase correction with adaptive equalizers are required to decrease these effects, as well as a careful choice of the frequency content of the signal to be transmitted.

On the contrary, for in-pipe acoustic communication, the distribution of the acoustic energy is affected by the pipe boundary, giving rise to a guided wave propagation, which results in an increased complexity in the description of the phenomenon. Hence the in-pipe waveguide requires more sophisticated modeling techniques, while for the open sea case geometric ray-tracing theory is sufficient to model the acoustic channel [12], [16]. Most theoretical analyses of guided wave propagation decompose the wave into various forms of propagation, which are called modes [6], [12], [17] and can be longitudinal, torsional and flexural in hollow, fluid-filled, elastic cylinders.

The problem is formally studied by deriving the wave equation for the pressure variations and finding its solutions. Different degrees of approximation can be employed with the most common approach being that of considering the perfectly rigid pipe case initially, and next the flexible pipe embedded in soil. The rigid pipe hypothesis can be suitable when the pipe wall material is much stiffer than the internal fluid, and the two have a large acoustic impedence difference [6], [12]. For this case it is found that a fundamental mode exists which travels in the axial direction and has wavefronts with constant phase across the cylinder cross section [12]. In addition, higher order modes, which are dispersive, arise as the frequency increases in a similar fashion to electromagnetic waveguides [18].

The model of flexible pipe embedded in soil takes into account the effect of pipe stiffness and soil properties. In this case wave energy can be radiated to the pipe wall and surrounding soil, causing additional attenuation and multipath propagation. The delayed arrivals of the propagating signal through different paths may overlap destructively, causing severe signal attenuation, also known as fading [12]. Moreover, the wave propagation properties are influenced by many physical parameters such as distance, pipe diameter, surrounding soil properties, damping, wall thickness, positioning of transmitter and receiver and so forth.

A number of publications have dealt with the in-pipe acoustic wave propagation for communication purposes. Among these, [4], [5], [9] employed waves in the ultrasonic range to induce an elastic wave in the pipe wall, while [6] provided an investigation on channel characterization for guided propagation in straight pipes. All provided practical implementations of the communication system, although the experimental demonstration was performed on a lab scaled version of a pipe in all cases. Mode-based analytical models were employed in [6] and [9] for the prediction of propagation phenomena. However, the proposed modeling is of limited practical utility due to the complex physical structure of real-world pipelines. In fact, mode-based models are usually derived for simple geometric cases, such as straight-line cylindrical pipes, while real-world pipelines are structurally very complex, since they can include joints, shafts, curves and branches. Moreover, even in cases of simple geometry, the propagation phenomena are largely dependent on the physical parameters of the pipe, such as the internal diameter, wall material and thickness, as well as on the properties of the surrounding soil, which might be unknown in practical cases.

To the authors' knowledge, the only large-scale communication system, based on acoustic wave propagation through a real-world pipeline is presented in [7]. The work reported on the design and implementation of a communication system over a distance of 70 m. The authors presented a characterization phase in which an optimal frequency of around 500 Hz was identified for the carrier frequency and different data modulation schemes were evaluated. However, the presented results for the channel response included the frequency response of the transducers, making it difficult to understand the frequency selectivity of the acoustic channel alone. Furthermore, the employed transducers were magnetically attached to the exterior of the pipe, which, although presenting the advantage of a non invasive installation, may not guarantee a good coupling of the actuator to the acoustic medium. Moreover, the noise floor was only 4 dB below the received signal, in only a narrow band, which may result in an unreliable communication.

The present work proposes a methodology that can be applied to the design of communication systems based on guided acoustic waves. A channel characterization procedure based on experimental measurements is presented, which can be used for modeling purposes and carrying out the system design. The proposed approach is presented in II, while in III its application to a case study is shown. A real-world UWSS was chosen in order to highlight the validity of the proposed approach. The experimental measurements performed for the channel characterization are then employed in III-B to build a black-box model of the channel, in order to enable the communication system simulation for the evaluation of different modulation schemes. This is presented in IV, where parametric simulations are performed in order to identify a suitable set of modulation parameters resulting in a low BER (Bit Error Rate) communication. Finally, in V the practical implementation of the communication system is described and experimental results are provided.

II. SYSTEM DESIGN METHODOLOGY

This section presents a new design procedure for the communication system, which is based on a model derived from experimental measurements of the communication channel.

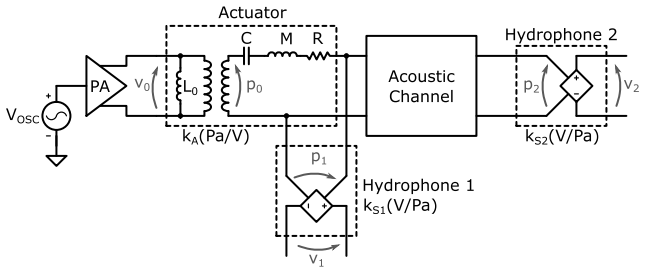

FIGURE 1. Schematic representation of the acoustic channel characterization system.

A. CHANNEL CHARACTERIZATION

The basic idea behind the acoustic channel characterization procedure is that of measuring the complex frequency response of the channel under examination, in a certain frequency range. Assuming the channel is a real-world pipeline, if two entry points are identified, it can be described by means of the relation existing between fluid properties at the ports of the system.

For a linear, time-invariant system, frequency domain characterization can be performed. The motivation behind frequency characterization is the complicated behavior of the guided wave propagation, which can present reflections, echoes etc. Characterization of the channel in the frequency domain allows one to account for all these effects, in the complex transfer characteristics of the channel.

The time-invariance assumption is justified by the fact that time variation of environmental variables is minimal in the pipeline, with only daily or seasonal temperature variations slightly affecting the channel properties [12].

The linearity assumption instead, is justified in what follows. The presence of a sound wave produces changes in density, pressure, and temperature in the fluid, of which the pressure changes are usually the most easily measurable [19]. Furthermore, as long as the pressure changes are small with respect to the equilibrium pressure in the fluid, the acoustic energy distribution in the medium is described by (1)

$$\begin{aligned} E_{\mathrm{p}} &= \frac{1}{2}\kappa p^2 \\ E_{\mathrm{k}} &= \frac{1}{2}\rho u^2 \end{aligned} \tag{1}$$

where E_{p} is the potential energy density, κ is the fluid compressibility, p is the pressure change caused by the sound, E_{k} is the kinetic energy density, ρ is the fluid density and u is the velocity change [19]. From (1), a similar structure results to the equations describing the energy density behavior for an electrical transmission line [18], suggesting that, by using suitable transducers, the pipe can be characterized in a similar way to electrical two-port networks, by means of its voltage transfer functions.

A schematic representation of the system for the characterization procedure is shown in Fig. 1. The acoustic channel to be characterized is represented as a generic two-port network, described by the pressures p_1 and p_2. The voltage to pressure transducer, named "Actuator", has the task of providing a pressure excitation for the probing of the system. It is represented by a generic two-port model relating electrical and acoustical quantities [20] and it can be described by (2) in the phasorial domain

$$\begin{cases} I_0 = \left(\frac{1}{sL_0} + \frac{A^2K_{\mathrm{A}}^2}{Z_{\mathrm{m}}}\right) V_0 - \frac{A^2K_{\mathrm{A}}}{Z_{\mathrm{m}}} p_0 \\ U_0 = -\frac{A^2K_{\mathrm{A}}}{Z_{\mathrm{m}}} V_0 + \frac{A^2}{Z_{\mathrm{m}}} p_0 \end{cases} \tag{2}$$

where V_0 and I_0 are the input voltage and current, respectively, while p_0 and U_0 are the pressure and volume velocity at the moving surface at the acoustical side of the actuator. L_0 represents the input inductance, while the transduction factor is given by K_{A} and A is the area of the moving surface applying work on the acoustic medium. Finally, Z_{m} is a mechanical impedance given by the series model

$$Z_{\mathrm{m}} = R + sM + \frac{1}{sC} \tag{3}$$

where M is the moving mass, R is the mechanical resistance modeling losses and C is the compliance or the reciprocal of the elastic constant. The pressure to voltage transducers are named "Hydrophone 1" and "Hydrophone 2", and are modeled as ideal dependent sources, with sensitivity k_{S1} and k_{S2}, respectively.

The characterization procedure allows one to get the complex frequency response points, which can be used in the subsequent channel modeling phase. The procedure is carried out by probing the channel at fixed frequencies, after selecting a set of M values, with step equal to Δf. Voltages $v_{\mathrm{i,m}}[n]$ are acquired with a sampling frequency f_{S}, where $i \in (0, 1, 2)$ is the voltage index, $m \in (0, 1, 2, \ldots, M-1)$ is the test frequency index and $n \in (0, 1, 2, \ldots, N-1)$ is the discrete-time index. The probing frequency step should be chosen so that it is an integer multiple of the frequency resolution, that is

$$\frac{\Delta f}{f_{\mathrm{S}}} N \in \mathbb{N}. \tag{4}$$

After sampling, the signals are elaborated by means of the Discrete Fourier Transform (DFT), yielding the frequency-domain sample arrays

$$V_{\mathrm{i,m}}[k] = \sum_{n=0}^{N-1} v_{\mathrm{i,m}}[n] \cdot e^{-\mathrm{j}\frac{2\pi}{N}kn} \tag{5}$$

where $k \in (0, 1, 2, \ldots, N-1)$ is the discrete-frequency index. The frequency-domain evaluation of the signal allows one to consider only the component at the frequency of interest (f_{m}), i.e. the one which has been excited by the actuator. The complex transfer function between the input voltage of the actuator and the output voltage of the second hydrophone can be evaluated as

$$H_{\mathrm{C}}[m] = \frac{V_{2,\mathrm{m}}[\bar{k}]}{V_{0,\mathrm{m}}[\bar{k}]} \in \mathbb{C}, \tag{6}$$

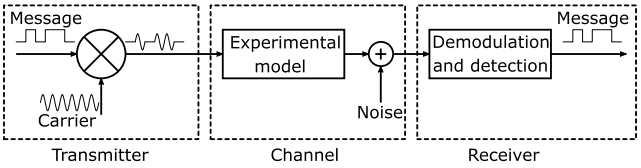

FIGURE 2. Block diagram of the communication system.

where

$$\bar{k} = \frac{\Delta f}{f_S} \cdot m \cdot N \tag{7}$$

is the index of the excited frequency. After evaluation, the probing frequency is increased and the procedure is repeated until the bandwidth of interest is covered. The presence of the hydrophone 1 allows for the evaluation of the pressure transfer function

$$H_P[m] = \frac{p_{2,m}[\bar{k}]}{p_{1,m}[\bar{k}]} = \frac{V_{2,m}[\bar{k}]}{V_{1,m}[\bar{k}]} \cdot \frac{k_{S1}}{k_{S2}} \in \mathbb{C}, \tag{8}$$

nulling the effect of the mechanical impedance of the actuator, which can be difficult to estimate.

B. CHANNEL MODELING

Using the frequency characterization data points, a model reproducing the input-output behavior of the system under examination can be built. One popular approach for modeling tabular frequency dependent data, without relying on a priori knowledge of the underlying system is vector fitting [21]. This method is well suited for fitting measured frequency domain responses by means of rational function approximations.

Given a set of frequency-domain complex samples, the vector fitting procedure allows one to find the approximating rational function

$$H(s) \simeq \sum_{q=1}^{Q} \frac{c_q}{s - a_q} + d + sh \tag{9}$$

where Q is the order of the approximating function, c_q and a_q are respectively residues and poles and d and h are real quantities. The found rational function minimizes the distance from the measurement data in the least squares sense.

C. DATA MODULATION SCHEME EVALUATION

Once completed the modeling of the transfer function, numeric simulations can be carried out in order to evaluate the performance of different modulation schemes, aiming at the identification of the most suitable one. A block diagram representation of the system to be simulated is shown in Fig. 2. Models for the transmitter and the receiver can be included in order to evaluate the overall performance of the communication system. The channel is represented by the experimentally built black-box model, with Additive White Gaussian Noise (AWGN) at its output, which is one of the most used models for communication channels [22]. A figure of merit such as the BER can then be evaluated as the parameters of the modulation are varied. Besides performance, other parameters such as power consumption and implementation complexity should be taken into account when selecting a certain modulation scheme for the communication system.

TABLE 1. Parameters of the pipeline under test.

Parameter	Value
Material	Polyethylene
Outer diameter	110 mm
Wall thickness	10 mm
L_1	73 m
L_2	165 m

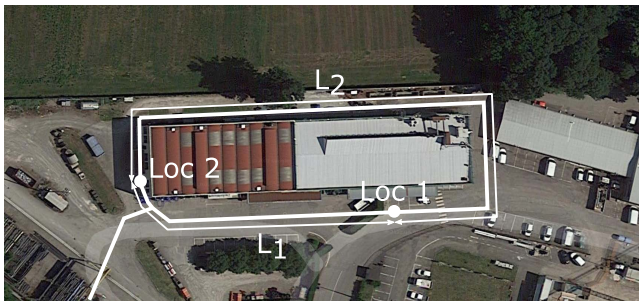

FIGURE 3. Top view of the test site. The pipeline is schematically shown by means of the white line while the position of the two access points is shown by the white dots.

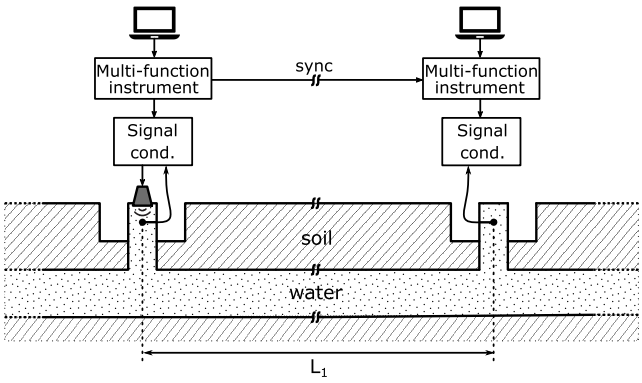

FIGURE 4. Experimental setup used for the channel characterization step. An excitation source is present at one end and two pressure transducers are acquired by means of two PC-based multi-function instruments.

III. CASE STUDY

The application of the proposed methodology to a practical case study is presented in what follows.

A. CHANNEL CHARACTERIZATION EXPERIMENTAL SETUP

The system under test was a water pipeline, a view from above of which is shown in Fig. 3. The pipeline under investigation has a near-rectangular shape and it is buried underground at a depth of about 1 m. Its physical properties are given in Table 1.

The characterization of the system under investigation was carried out in a frequency range of (40 Hz, 200 Hz), which

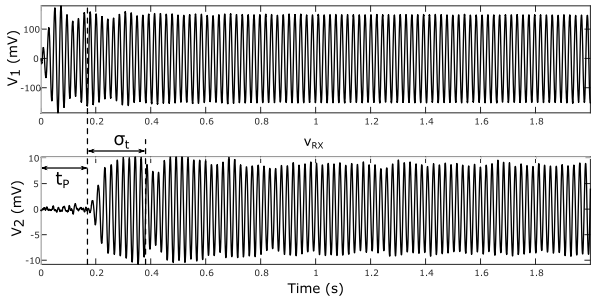

FIGURE 5. Single frequency signal at the (top) transmitter and at the (bottom) receiver. The 47 Hz case is shown and the gain of the conditioning amplifiers has been removed.

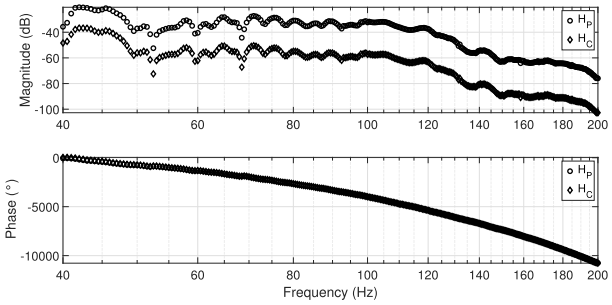

FIGURE 6. Measured magnitude and phase of the two transfer functions $H_C(s)$ and $H_P(s)$.

was selected based on the frequency response of the actuator. The experimental setup used for the channel characterization can be seen in Fig. 4. The number of samples for each acquisition was $N = 8000$ and the sampling frequency $f_S = 4\,\text{kHz}$, resulting in a frequency step of 0.5 Hz. In Fig. 5 waveforms at single frequency at the transmitter and at the receiver are shown for the case of a 47 Hz frequency. From the time-domain waveforms the propagation time of the signal can be noticed, which has been indicated as t_P in Fig. 5. The signal propagation speed can be computed in this case, as the length of the shortest path is known, i.e.,

$$c = \frac{L_1}{t_P} = \frac{73\,\text{m}}{170\,\text{ms}} = 429\,\text{m/s}. \tag{10}$$

This result is in good agreement with measurements from [23] for buried polyethylene pipes. Since the length of the secondary path is also known in this case, the secondary fly time can be evaluated as

$$t_{P,\text{sec}} = \frac{L_2}{c} = \frac{165\,\text{m}}{429\,\text{m/s}} = 384\,\text{ms}. \tag{11}$$

This time instant corresponds to a second arrival which can be noticed in the received signal. The distance between the two arrivals has been marked as σ_t in Fig. 5 and equals 214 ms. By carrying out the measurement process for every frequency point, the plots of Fig. 6, representing the behavior of the transfer functions defined in II-A, can be built. Referring to Fig. 1, two identical hydrophones were employed for

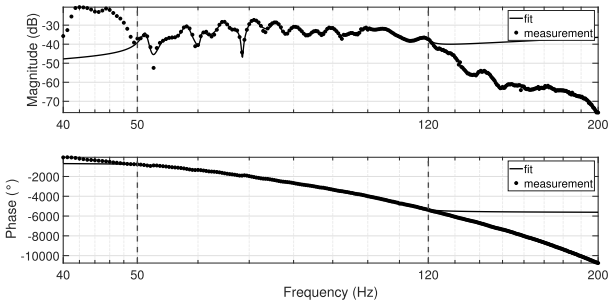

FIGURE 7. Magnitude and phase fitting of $H_P(s)$ with an order of 38.

measuring the pressures p_1 and p_2, so that

$$k_{S1} = k_{S2} \tag{12}$$

and the pressure transfer function of the pipeline is given by

$$H_P[m] = \frac{V_{2,m}[\bar{k}]}{V_{1,m}[\bar{k}]} \cdot \frac{k_{S1}}{k_{S2}} = \frac{V_{2,m}[\bar{k}]}{V_{1,m}[\bar{k}]}. \tag{13}$$

By comparison between the two transfer functions it results that the pipe is the main responsible for the frequency-dependent attenuation, while the transducers account for an attenuation factor with a slight frequency dependence.

A low-pass behavior of the channel frequency response can be noticed, with the magnitude decreasing for frequencies above 120 Hz. Below 120 Hz, the magnitude shows a highly frequency-selective behavior with several deep notches, reflecting the multipath propagation characteristics observed in the time domain. Fig. 6 also shows a less attenuated band between 40 Hz and 50 Hz, which, however, corresponds to a frequency range in which the actuator does not operate in an efficient manner.

B. MODEL BUILDING AND VALIDATION

Channel modeling was performed by fitting the acquired frequency-domain data with two rational functions, in order to derive the complex transfer functions $H_C(s)$ and $H_P(s)$. In accordance with the measurement results previously presented, a frequency interval (50 Hz, 120 Hz) was chosen for the fitting with model orders of $Q_C = 42$ and $Q_P = 38$, which showed to be sufficient for a good approximation of both magnitude and phase. The fitting result is shown in Fig. 7 for $H_P(s)$. An analysis of the singularities showed that all poles are in the left half of the complex plane for both models.

The derived model was validated by comparison of measurement and time-domain simulation, with an amplitude modulated signal at the input. The carrier frequency was set to 71 Hz, which corresponds to a local maximum of the transfer function, and the comparison results are shown in Fig. 8. Transient simulations were performed by feeding at the system input the measured input signal of the actuator. In general, a good agreement is achieved between the simulated and the measured signals. In particular, although the signal at the far end hydrophone has some slight amplitude mismatch (v_2), the model correctly predicts the arrival of both

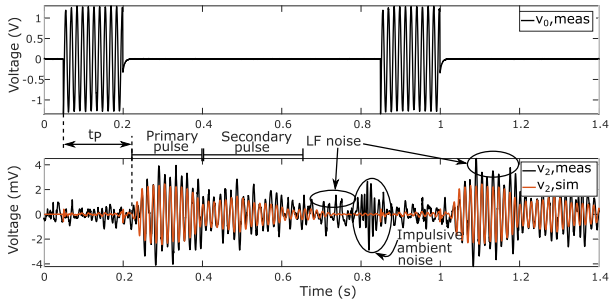

FIGURE 8. Model validation by comparing numerical simulation and measurement results. (Top) signal at the input of the actuator - v_0, and (bottom) raw signal at the output of the far end hydrophone - v_2, compared to simulation result.

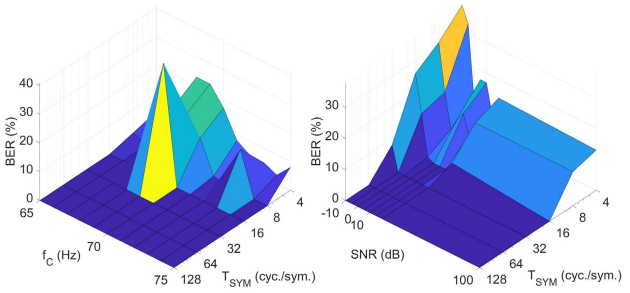

FIGURE 9. BER simulation for the OOK scheme, (left) SNR = 10 dB, $T_{HIGH} = T_{SYM}$, (right) $f_C = 71$ Hz, $T_{HIGH} = T_{SYM}$.

the primary and secondary pulses through the two propagation paths. The irregular magnitude mismatch is likely due to the superposition of low frequency noise onto the measured signal, which can be ascribed to environmental noise.

IV. COMMUNICATION LAYER SIMULATION

The extracted model enables the simulation of data transmission over the characterized channel with the aim of evaluating the performance of various modulation schemes. Popular data modulation techniques used in previous works, based on acoustic guided wave propagation [4], [5], [7], [9], are the binary digital modulations such as Amplitude Shift Keying (BASK), Frequency Shift Keying (BFSK) and Phase Shift Keying (BPSK), or their variations. While binary modulations provide the lowest bandwidth efficiency, carrying just one bit per symbol, they require a lower complexity than M-ary schemes to be implemented. On vice versa, the symbols are maximally spread for binary modulations, which increases the robustness to noise of the modulated signal. The complexity element is an important one in view of a low-cost and low-power system implementation. Indeed, as the complexity of the communication scheme increases, so does the performance of the required elaboration units needed for its implementation. Hence, when choosing the scheme to be used, a trade off has to be made between performance and complexity.

A simulation bench was built in Matlab, for the performance evaluation of the BASK, BFSK and BPSK data modulation schemes, which included a modulation block, the experimentally obtained channel model and a demodulation block. The BER was evaluated as parameters such as the carrier frequency f_C, symbol time duration T_{SYM} and added noise level were varied. Another degree of freedom was added by allowing the carrier duration, in correspondence of the "one" symbol, to be different from the symbol time, with $T_{HIGH} \leq T_{SYM}$. The BER was evaluated after applying a sequence of 100 casually generated symbols at the channel input. Results of BER simulations for the ASK scheme, in its On-Off Keying (OOK) version, following parameters sweep, are presented in Fig. 9. The demodulation in this case was performed in a non coherent fashion, by energy detection and threshold comparison. The carrier frequency was swept inside the modeled range and the symbol time duration was varied from 4 to 128 carrier cycles per symbol. Simulation results showed that the BER is virtually zero for longer symbol times, independently from the carrier frequency choice. This is in good agreement with the nature of the available channel, which exhibited the multipath fading characteristics in its transfer function. It is understood that increasing the symbol duration beyond the coherence bandwidth of the channel results in lower BER [22]. At shorter symbol time duration, the small coherence bandwidth of the channel would require equalization in order to compensate for the non flat channel transfer function. Although selecting a longer symbol time reduces the BER, this choice also lowers the symbol-rate, which for binary modulations is the same as the bit-rate and is defined as

$$\mathrm{BR} = \frac{1}{T_{\mathrm{SYM}}}. \tag{14}$$

At lower symbol time duration the BER varied with the carrier frequency and it was larger for frequencies at which the magnitude of the transfer function is smaller, such as the 69 Hz case. The effect of the additive white noise at the channel output, after fixing the carrier frequency at 71 Hz, at various symbol time duration, can also be observed in Fig. 9. The BER increased as the added noise level increased, while the behavior as a function of the symbol time duration was similar to the previous case, meaning that shorter symbol duration led to larger BER. Finally, the BER behavior as a function of the symbol duration was investigated, while varying also the duration of T_{HIGH}. The simulation results are plotted in Fig. 10. The SNR was fixed at -5 dB in order to avoid a low error rate at higher SNR. Results showed that the BER was virtually zero for symbol duration longer than 32 cycles of carrier frequency. For shorter symbol duration the BER was the lowest if $T_{HIGH} = 0.5 \cdot T_{SYM}$. The observation of the probable symbols after demodulation, prior to bit detection, revealed that the BER improvement for the case $T_{HIGH} = 0.5 \cdot T_{SYM}$ is related to the reduction of Inter-Symbol Interference (ISI), which is caused by the secondary propagation path. Indeed, at $T_{HIGH} = T_{SYM}$, every time a "1-0" sequence is present, the "1" symbol interferes with the subsequent "0", causing the error probability at the receiver to increase. The choice $T_{HIGH} = 0.5 \cdot T_{SYM}$ showed to be a good trade-off

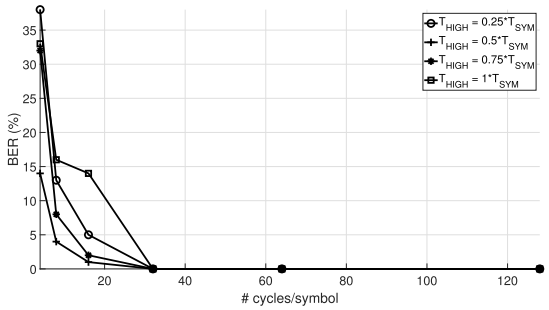

FIGURE 10. BER simulation for the OOK scheme, SNR = −5 dB, f_C = 71 Hz.

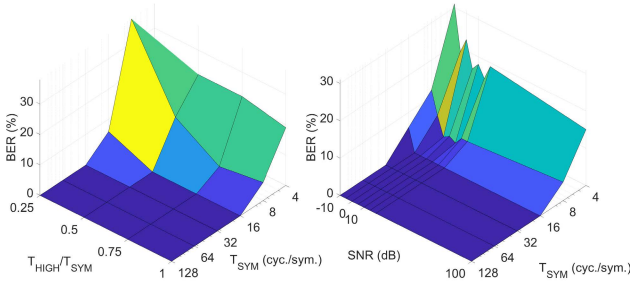

FIGURE 11. BER simulation for the BFSK scheme with f_{C1} = 65 Hz, f_{C2} = 75 Hz, (left) SNR = 10 dB, (right) $T_{HIGH} = T_{SYM}$.

between ISI reduction and strength of the primary pulse, which should be detected. Furthermore, decreasing T_{HIGH} while keeping T_{SYM} fixed, has the advantage of lowering the energy needed for the transmission, which lowers the overall power consumption of the system. Simulations were carried out in a similar way for the BFSK scheme in which the carrier frequencies were fixed at 65 Hz and 75 Hz and the other parameters were swept. The demodulation was performed in non coherent fashion, following two bandpass filters centered at the carrier frequencies. The resulting BER, as the parameters were swept, is shown in Fig. 11. The results look similar to those obtained with the OOK modulation, as far as the SNR − T_{SYM} is concerned, with the largest error rate corresponding to large noise levels and short symbol time duration. On the other hand, a decreasing T_{HIGH} did not result in lower BER. This is due to the representation of both symbols with a sinusoidal pulse, which reduces the severity of the ISI as the bits are detected by means of threshold comparison. Finally, the performance of the BPSK was evaluated. In this case the demodulation was performed in coherent fashion, assuming the recovery of a synchronized local carrier is possible. BER results, as the parameters were swept, are represented in Fig. 12. Results showed a reduced sensitivity of the BER with respect to the carrier frequency choice, as compared to the OOK case. Also, the absolute error figures were much lower, as compared to the other modulation schemes. This is likely related to the demodulation, since it is generally accepted that coherent demodulation yields better performance as compared to non coherent one [22]. It can also be observed that, at fixed carrier frequency, the BER is virtually zero as the SNR, shown in Fig. 12, was swept. It appears

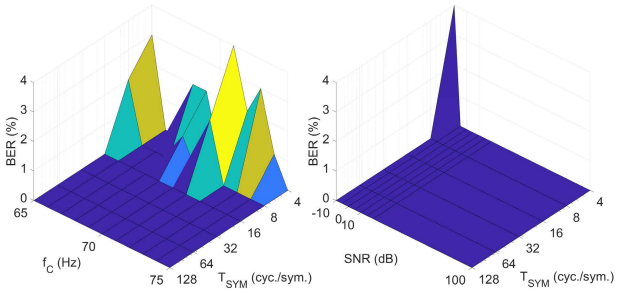

FIGURE 12. BER simulation for the BPSK scheme, (left) SNR = 10 dB, $T_{HIGH} = T_{SYM}$, (right) f_C = 71 Hz, $T_{HIGH} = T_{SYM}$.

from these simulations that, among the simple binary modulation schemes, the BPSK has the best performance, in terms of BER. However, this scheme requires the most complex demodulation technique, in which the carrier recovery has to be performed. The other two schemes, on the other hand, showed similar performance, with the BFSK presenting the drawback of requiring two bandpass filtering blocks in the demodulator, as compared to the one required by the OOK. These schemes are more suitable for software implementation on board of low-cost and low-power microcontrollers, which typically have reduced computational capabilities. It was also observed that the ISI-related errors can be mitigated in the OOK scheme by reducing the carrier-on duration in the "1" symbol.

V. SYSTEM IMPLEMENTATION

The detailed description of the communication system implementation, according to the proposed methodology, is presented in this section.

A. NOISE CHARACTERIZATION

Noise measurements were carried out for an extended period of time, aiming to understand the ambient noise levels in a real-world pipeline, which is the one presented in III. The measurement system in this case only included a hydrophone and relative signal acquisition circuitry, placed at "Loc 1" in Fig. 3. The hydrophone had a sensitivity of $S = -80$ dB rel V/Pa. Data records of 2^{14} samples with a sampling rate of $f_S = 4.4$ kHz were acquired periodically and transferred to a remote server for later processing. The acquired data records were then analyzed through the DFT in order to assess the energy distribution of the noise inside the considered bandwidth. Some of the loudest acquisitions in a 10-day period are represented in Fig. 13. It results that the most noisy frequency band is the one between 10 Hz and 200 Hz, with the observed noise magnitude in the interval (−80 dBV/NBW, −60 dBV/NBW), where the noise bandwidth is NBW = 0.405 Hz. In the spectra, the presence of the odd harmonics from the mains can also be noticed.

B. HARDWARE DESIGN

Conversely from several other works [6], [7], in which piezoelectric actuators were employed, a solenoid transducer was

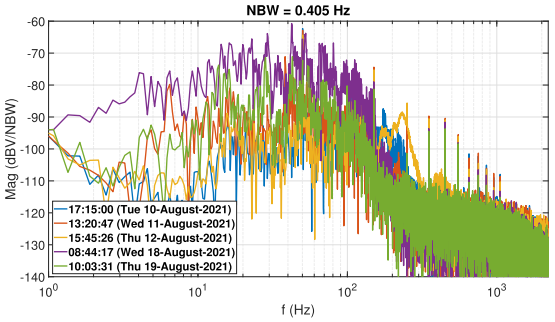

FIGURE 13. Some of the loudest noise records in a 10-day period, along with the acquisition dates.

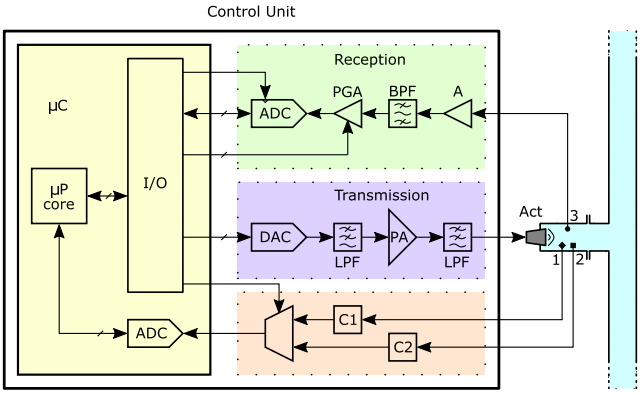

FIGURE 14. Block diagram of the single node. 1 - temperature sensor, 2 - static pressure sensor, 3 - hydrophone. Blocks C1 and C2 represent conditioning circuitry for the measurement of temperature and hydrostatic pressure, respectively.

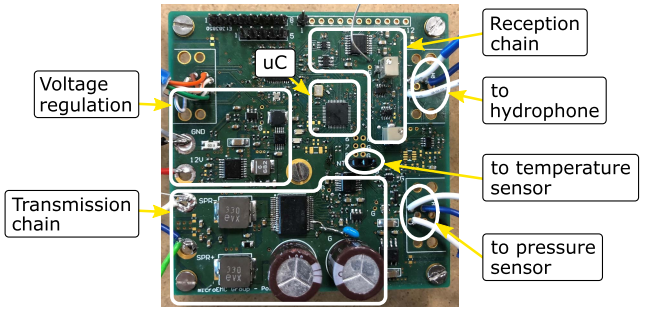

FIGURE 15. Picture of the node Electronic Control Unit (ECU).

used here. The main reason for this is the low frequency of operation, allowing for the generation of low frequency waves, which are more suitable for long distance propagation inside pipes [12].

Based on the noise observations previously shown, a worst-case acquisition was considered, which showed an RMS value of $e_{\mathrm{n,RMS}} = 3.7\,\mathrm{mV}$ across the whole Nyquist bandwidth. According to the hydrophone sensitivity, the equivalent pressure noise inside the pipe results

$$p_{\mathrm{n,RMS}} = \frac{e_{\mathrm{n,RMS}}}{S} = 37\,\mathrm{Pa}. \tag{15}$$

Fixing a Signal to Noise ratio (SNR) of 20 dB, in the worst case, yields the pressure signal magnitude that is needed at the hydrophone, as

$$p_{\mathrm{rx,RMS}} = 10 \cdot p_{\mathrm{n,RMS}} = 370\,\mathrm{Pa}, \tag{16}$$

which corresponds to a received voltage $v_{\mathrm{rx,RMS}} = 37\,\mathrm{mV}$. Previous research related to the acoustic wave propagation in buried pipes showed that attenuation values for the fundamental propagation mode can be between 0.05 dB/m and 0.23 dB/m [24], [25], [26] and a reasonable value of $\alpha = 0.2\,\mathrm{dB/m}$ is assumed in what follows. Hence, being the transmitter-receiver distance $L_1 = 73\,\mathrm{m}$, the pressure that should be generated at the transmitting side results

$$p_{\mathrm{tx,RMS}} = p_{\mathrm{rx,RMS}} \cdot 10^{\frac{\alpha L}{20\,\mathrm{dB}}} \simeq 2\,\mathrm{kPa}, \tag{17}$$

which, for a circular radiating surface with radius $r = 20\,\mathrm{mm}$, corresponds to a force of $F_{\mathrm{tx,RMS}} = 2.5\,\mathrm{N}$.

As far as the signal acquisition is concerned, the noise specification of the employed hydrophone is $e_{\mathrm{n,h,RMS}} = 12\,\mu\mathrm{V}$, which yields a dynamic range of

$$\mathrm{DR} = 20 \cdot \log\left(\frac{37\,\mathrm{mV}}{12\,\mu\mathrm{V}}\right) = 70\,\mathrm{dB} \tag{18}$$

for the measurement chain.

C. SYSTEM OPERATION DESCRIPTION

The developed communication system consists of two identical nodes, which are represented by the block diagram in Fig. 14. The block diagram shows that each node contains both acquisition and generation chains, hence being able to achieve bidirectional communication. The operation is governed by a general purpose microcontroller, which manages signal acquisition and generation, as well as the acquisition of other quantities such as water temperature and pressure. A photograph of one of the developed modules can be seen in Fig. 15. Although the BPSK modulation scheme showed good performance in the simulation phase, the implementation of the coherent detection proved difficult in the presence of large noise levels and at such low carrier frequency. Aiming at implementing the scheme on board a low-cost microcontroller, a non coherent demodulation was chosen, while the modulation scheme was the OOK, due to its simpler implementation and reduced energy demands with respect to the BFSK. A block diagram of the complete communication system is shown in Fig. 16, while a picture of one of the nodes mounted onto the plant can be seen in Fig. 17.

D. EXPERIMENTAL RESULTS

Experimental communication tests were performed at the same test site as in III. Two nodes were mounted, specifically, "Node 1" and "Node 2" of Fig. 16 at "Loc 1" and "Loc 2" of Fig. 3, respectively. OOK data modulation was performed with $f_C = 71\,\mathrm{Hz}$, $T_{\mathrm{SYM}} = 400\,\mathrm{ms}$ and $T_{\mathrm{HIGH}} = 150\,\mathrm{ms}$ and the data packet had the structure shown in Fig. 18. A record of the received signal at various stages of the demodulation chain, as presented in Fig. 16, is shown in Fig. 19. It can be

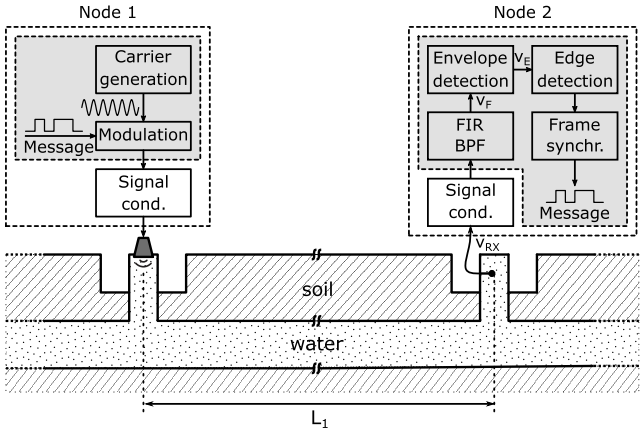

FIGURE 16. Block diagram of the communication system. The shaded rectangles represent software blocks. Node 1 is shown in transmitter mode, while Node 2 in receiver mode.

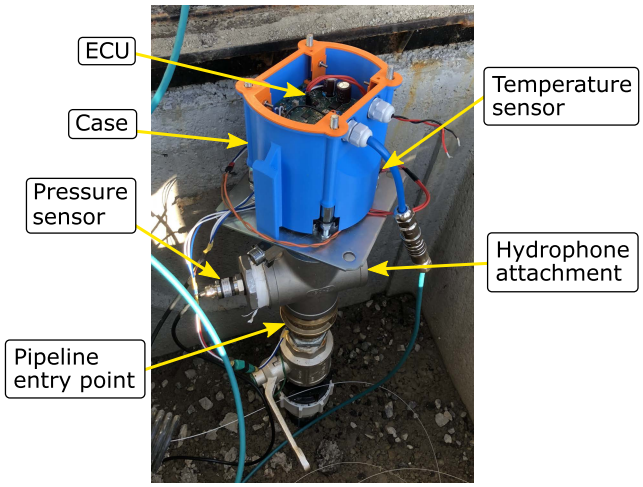

FIGURE 17. One of the developed nodes mounted onto the water pipe. The actuator is covered by the case, underneath the ECU.

1	01010101	idField Byte	data0 Byte	data1 Byte	CRC Byte	1

FIGURE 18. Structure of the data packet. Two ones are inserted at the head and tail of the packet. A byte is added at the beginning for the frame synchronization at the receiver.

seen that the received signal is affected by a large amount of noise, while after the bandpass filtering stage the two pulses carried by the central frequency of the filter are clearly visible. The signal at the output of the peak detection stage is then compared to the threshold in order to locate the pulse transitions.

Bidirectional data communication was successfully achieved across the 73 m section of the water distribution pipe. "Node 1" issued a data request command, which was correctly received by "Node 2". Measurement of the water temperature and static pressure were then performed and the data was sent back to the requesting node. The bitrate was 2.5 bps and a data packet with the structure shown in Fig. 18 required 16.8 s for the transmission to be completed.

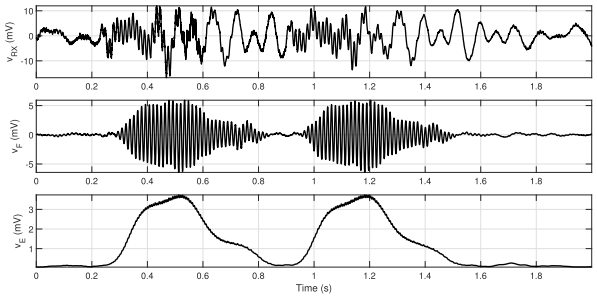

FIGURE 19. (Top) Received signal - v_{RX}, (middle) filtered signal - v_F, (bottom) envelope signal - v_E.

Although the transfer function of the channel can be time-variant, due to the temperature dependence of the water properties [19], communication tests performed in December 2021 and April 2022, with environmental temperatures of 5 °C and 17 °C, respectively, resulted in successful data transmission.

VI. CONCLUSION

This work reported on a design approach for communication systems based on guided pressure waves in fluid-filled pipelines. The proposed methodology is based on the experimental characterization of the plant, prior to the system design, by measuring the pressure transfer function between two ports of the system. The characterization technique was applied to a practical case study and the results highlighted the dispersive nature of the acoustic channel. The collected data was then employed in the building of a black-box model, which was used for the data modulation simulation. The simulations showed a high dependence of the data modulation schemes on parameters such as the carrier frequency and the symbol time duration. In particular, the carrier frequency should be selected far from the notches present in the pressure transfer function, while the symbol time duration should be long enough to cope with the small coherence bandwidth of the channel. A reduction of the carrier-on duration also showed beneficial effects in reducing the effect of the multipath propagation. Finally, a practical implementation of the communication system was presented and experimental results showed the effectiveness of the proposed approach.

REFERENCES

[1] N. W. Damiano, L. Yan, B. Whisner, and C. Zhou, "Simulation and measurement of through-the-earth, extremely low-frequency signals using copper-clad steel ground rods," *IEEE Trans. Ind. Appl.*, vol. 53, no. 5, pp. 5088–5095, Sep. 2017, doi: 10.1109/TIA.2017.2703625.

[2] L. Yan, J. A. Waynert, and C. Sunderman, "Measurements and modeling of through-the-earth communications for coal mines," *IEEE Trans. Ind. Appl.*, vol. 49, no. 5, pp. 1979–1983, Sep./Oct. 2013, doi: 10.1109/TIA.2013.2260116.

[3] J. Li, M. A. Reyes, N. W. Damiano, B. G. Whisner, and R. J. Matetic, "Medium-frequency signal propagation characteristics of a lifeline as a transmission line in underground coal mines," *IEEE Trans. Ind. Appl.*, vol. 52, no. 3, pp. 2724–2730, May 2016, doi: 10.1109/TIA.2016.2517599.

[4] A. Heifetz, D. Shribak, X. Huang, B. Wang, J. Saniie, J. Young, S. Bakhtiari, and R. B. Vilim, "Transmission of images with ultrasonic elastic shear waves on a metallic pipe using amplitude shift keying protocol," *IEEE Trans. Ultrason., Ferroelectr., Freq. Control*, vol. 67, no. 6, pp. 1192–1200, Jun. 2020, doi: 10.1109/TUFFC.2020.2968891.

[5] S. Chakraborty, G. J. Saulnier, K. W. Wilt, E. Curt, H. A. Scarton, and R. B. Litman, "Low-power, low-rate ultrasonic communications system transmitting axially along a cylindrical pipe using transverse waves," *IEEE Trans. Ultrason., Ferroelectr., Freq. Control*, vol. 62, no. 10, pp. 1788–1796, Oct. 2015, doi: 10.1109/TUFFC.2015.007078.
[6] L. Jing, Z. Li, Y. Li, and R. Murch, "Channel characterization of acoustic waveguides consisting of straight gas and water pipelines," *IEEE Access*, vol. 6, pp. 6807–6819, 2018, doi: 10.1109/ACCESS.2018.2793299.
[7] K. M. Joseph, T. Watteyne, and B. Kerkez, "Awa: Using water distribution systems to transmit data," *Trans. Emerg. Telecommun. Technol.*, vol. 29, no. 1, p. e3219, Jan. 2018, doi: 10.1002/ett.3219.
[8] N. Saeed, A. Celik, T. Y. Al-Naffouri, and M.-S. Alouini, "Underwater optical wireless communications, networking, and localization: A survey," *Ad Hoc Netw.*, vol. 94, Nov. 2019, Art. no. 101935, doi: 10.1016/j.adhoc.2019.101935.
[9] S. He, N. Wang, M. Ho, J. Zhu, and G. Song, "Design of a new stress wave communication method for underwater communication," *IEEE Trans. Ind. Electron.*, vol. 68, no. 8, pp. 7370–7379, Aug. 2021, doi: 10.1109/TIE.2020.3003634.
[10] R. Long, P. Cawley, and M. Lowe, "Acoustic wave propagation in buried iron water pipes," *Proc. Roy. Soc. London A, Math., Phys. Eng. Sci.*, vol. 459, no. 2039, pp. 2749–2770, Nov. 2003, doi: 10.1098/rspa.2003.1148.
[11] M. Chitre, S. Shahabudeen, and M. Stojanovic, "Underwater acoustic communications and networking: Recent advances and future challenges," *Mar. Technol. Soc. J.*, vol. 42, no. 1, pp. 103–116, Mar. 2008, doi: 10.4031/002533208786861263.
[12] G. Kokossalakis, "Acoustic data communication system for in-pipe wireless sensor networks," M.S. thesis, Massachusetts Inst. Technol., Cambridge, MA, USA, 2006. [Online]. Available: https://dspace.mit.edu/handle/1721.1/34379
[13] M. Stojanovic and P.-P. J. Beaujean, "Acoustic communication," in *Springer Handbook of Ocean Engineering* (Springer Handbooks), M. R. Dhanak and N. I. Xiros, Eds. Cham, Switzerland: Springer, 2016, pp. 359–386.
[14] S. Güzelgöz, S. Yarkan, and H. Arslan, "Investigation of time selectivity of wireless channels through the use of RVC," *Measurement*, vol. 43, no. 10, pp. 1532–1541, Dec. 2010, doi: 10.1016/j.measurement.2010.08.020.
[15] S. Yarkan and H. Arslan, "Exploiting location awareness toward improved wireless system design in cognitive radio," *IEEE Commun. Mag.*, vol. 46, no. 1, pp. 128–136, Jan. 2008, doi: 10.1109/MCOM.2008.4427241.
[16] R. F. Ormondroyd, "A robust underwater acoustic communication system using OFDM-MIMO," in *Proc. OCEANS, Eur.*, Jun. 2007, pp. 1–6, doi: 10.1109/OCEANSE.2007.4302422.
[17] L. Jing, Y. Li, and R. D. Murch, "Wideband modeling of the acoustic water pipe channel," in *Proc. OCEANS, Shanghai*, Apr. 2016, pp. 1–8, doi: 10.1109/OCEANSAP.2016.7485640.
[18] D. M. Pozar, *Microwave Engineering*, 4th ed. Hoboken, NJ, USA: Wiley, 2012.
[19] P. M. Morse and K. U. Ingard, *Theoretical Acoustics*. Princeton, NJ, USA: Princeton Univ. Press, 1986.
[20] J. L. Butler and C. H. Sherman, *Transducers and Arrays for Underwater Sound* (Modern Acoustics and Signal Processing). Cham, Switzerland: Springer, 2016.
[21] B. Gustavsen and A. Semlyen, "Rational approximation of frequency domain responses by vector fitting," *IEEE Trans. Power Del.*, vol. 14, no. 3, pp. 1052–1061, Jul. 1999, doi: 10.1109/61.772353.
[22] E. McCune, *Practical Digital Wireless Signals* (The Cambridge RF and Microwave Engineering Series), 1st ed. Cambridge, U.K.: Cambridge Univ. Press, 2010.
[23] T. Graf, T. Gisler, P. Sollberger, and O. Schaelli, "Acoustic wave propagation in water filled buried polyethylene pipes," in *Proc. COMSOL Conf. Cambridge*, Cambridge, U.K., 2014, pp. 1–7.
[24] I. L. Vér and L. L. Beranek, Eds., *Noise and Vibration Control Engineering: Principles and Applications*, 2nd ed. Hoboken, NJ, USA: Wiley, 2006.
[25] M. Long, "Sound attenuation in ducts," in *Architectural Acoustics*. Amsterdam, The Netherlands: Elsevier, 2014, pp. 529–559.
[26] R. Long, M. Lowe, and P. Cawley, "Attenuation characteristics of the fundamental modes that propagate in buried iron water pipes," *Ultrasonics*, vol. 41, no. 7, pp. 509–519, Sep. 2003, doi: 10.1016/S0041-624X(03)00166-5.

MARKELJAN FISHTA (Member, IEEE) received the M.Sc. degree in electronic engineering from the Politecnico di Torino, Turin, Italy, in 2019, where he is currently pursuing the Ph.D. degree. In 2019, he joined the Department of Electronics and Telecommunication, Politecnico di Torino. His research interests include underwater communications, analog circuit design, and EMC issues.

ERICA RAVIOLA (Member, IEEE) was born in Asti, Italy, in 1993. She received the M.Sc. and Ph.D. degrees in electronic engineering from the Politecnico di Torino, Turin, Italy, in 2017 and 2021, respectively. She is currently a Researcher at the Politecnico di Torino. Her research interests include power electronics analysis and design, electromagnetic compatibility, and the Internet of Things application.

FRANCO FIORI (Member, IEEE) received the Ph.D. degree in electronic engineering from the Polytechnic University of Torino, Turin, Italy, in 1997. From 1997 to 1998, he was with the Research and Development EMC Group, STMicroelectronics, Milan, Italy, as a Leader. In 1999, he joined as a Researcher with the Polytechnic University of Torino, where he is currently a Professor in electronics and the Scientific Director of the Microelectronics EMC Laboratory. In his academic career, he has served as a PI in several national and international research projects, mostly on chip level EMC and power electronics. He has authored or coauthored more than 200 papers published in international journals and conference proceedings. His research interests include analog circuit design, power electronics, smart power devices, and electromagnetic compatibility.

Open Access funding provided by 'Politecnico di Torino' within the CRUI CARE Agreement